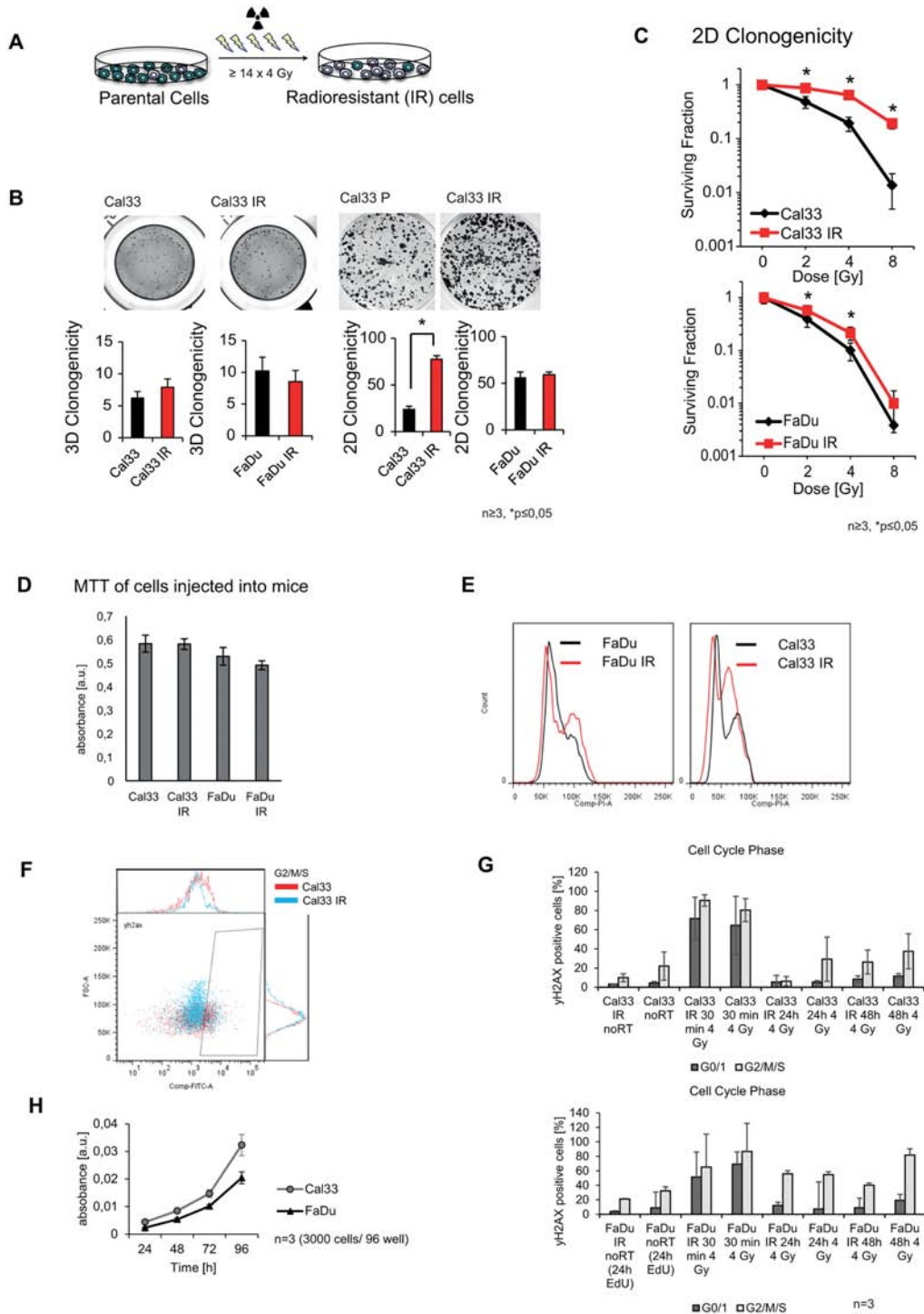
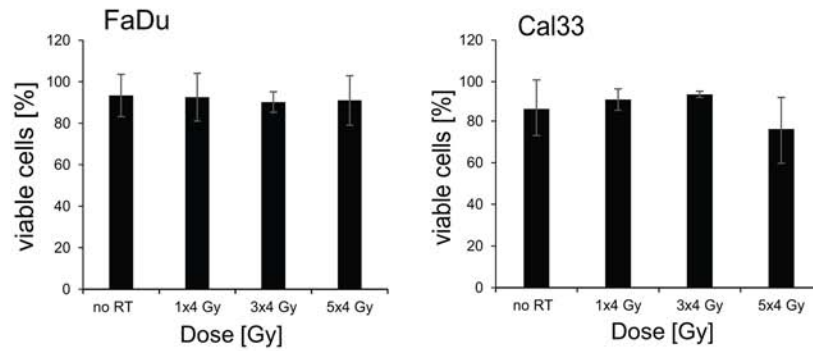


SUPPLEMENTARY FIGURES

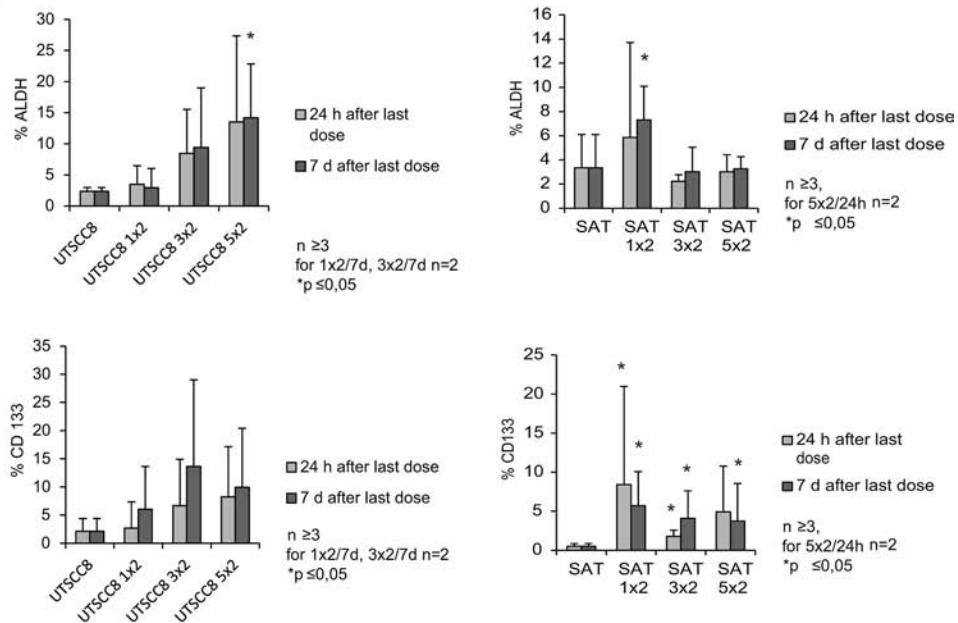


**Supplementary Figure S1: Establishment and characterization of irradiated HNSCC sublines.** A. IR sublines were established by repetitive irradiation of minimum 14 fractions of 4 Gy. B. Clonogenicity of FaDu and Cal33 parental versus IR sublines. C. 2D radiobiological survival assay of Cal33 and FaDu parental versus IR sublines. D. Viability of the cells injected into mice measured by MTT assay. E. DNA content measurement comparing parental and IR sublines of FaDu and Cal33. F. flow cytometric dot blot comparing  $\gamma$ H2AX foci positive cells of parental and IR Cal33 sublines in the G2/M phase of the cell cycle. G. distribution of  $\gamma$ H2AX foci positive cells in the cell cycle phases at different time points after irradiation. H. proliferation of Cal33 and FaDu cells measured at different time points after plating 3000 cell/ 96-well. ( $n \geq 3, p < 0,05$ , error bars = SD)

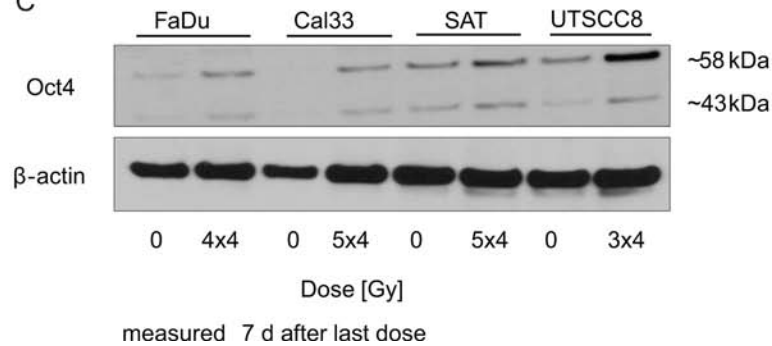
A



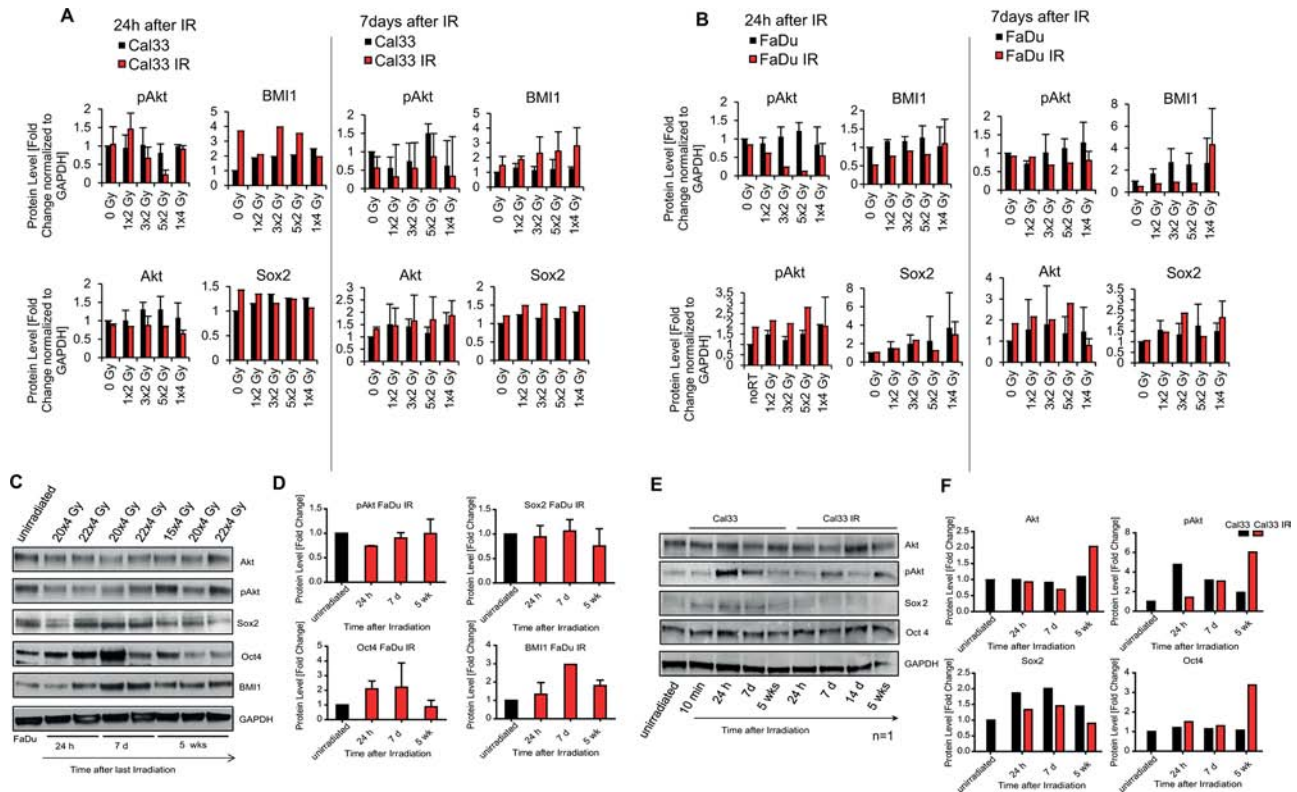
B



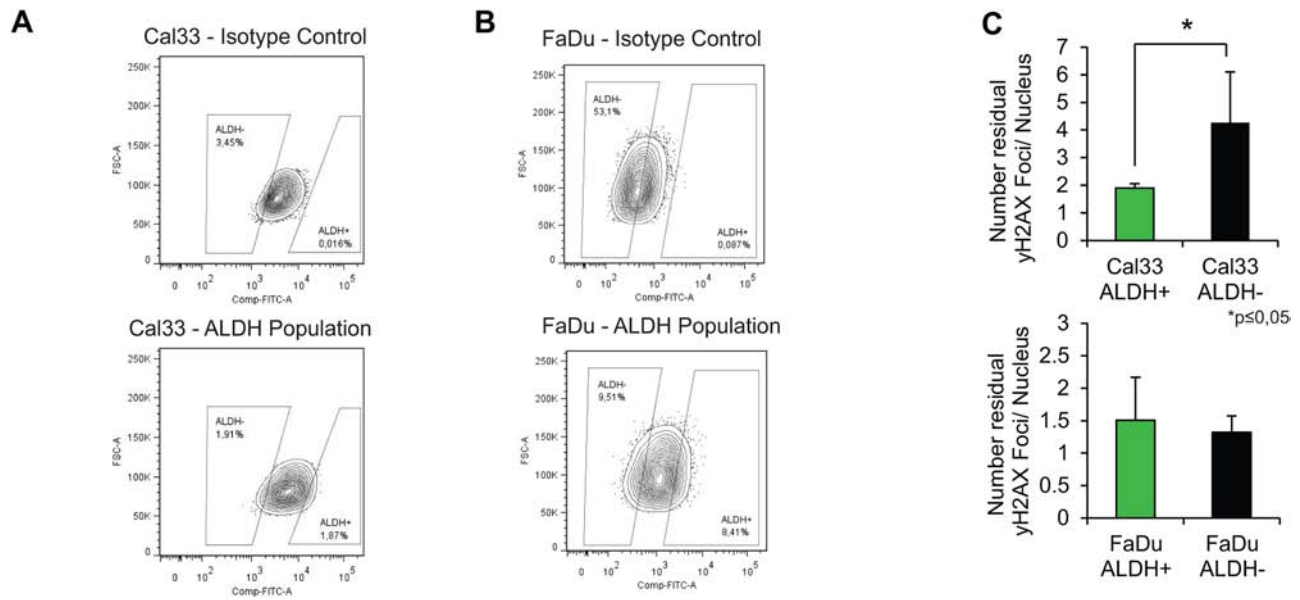
C



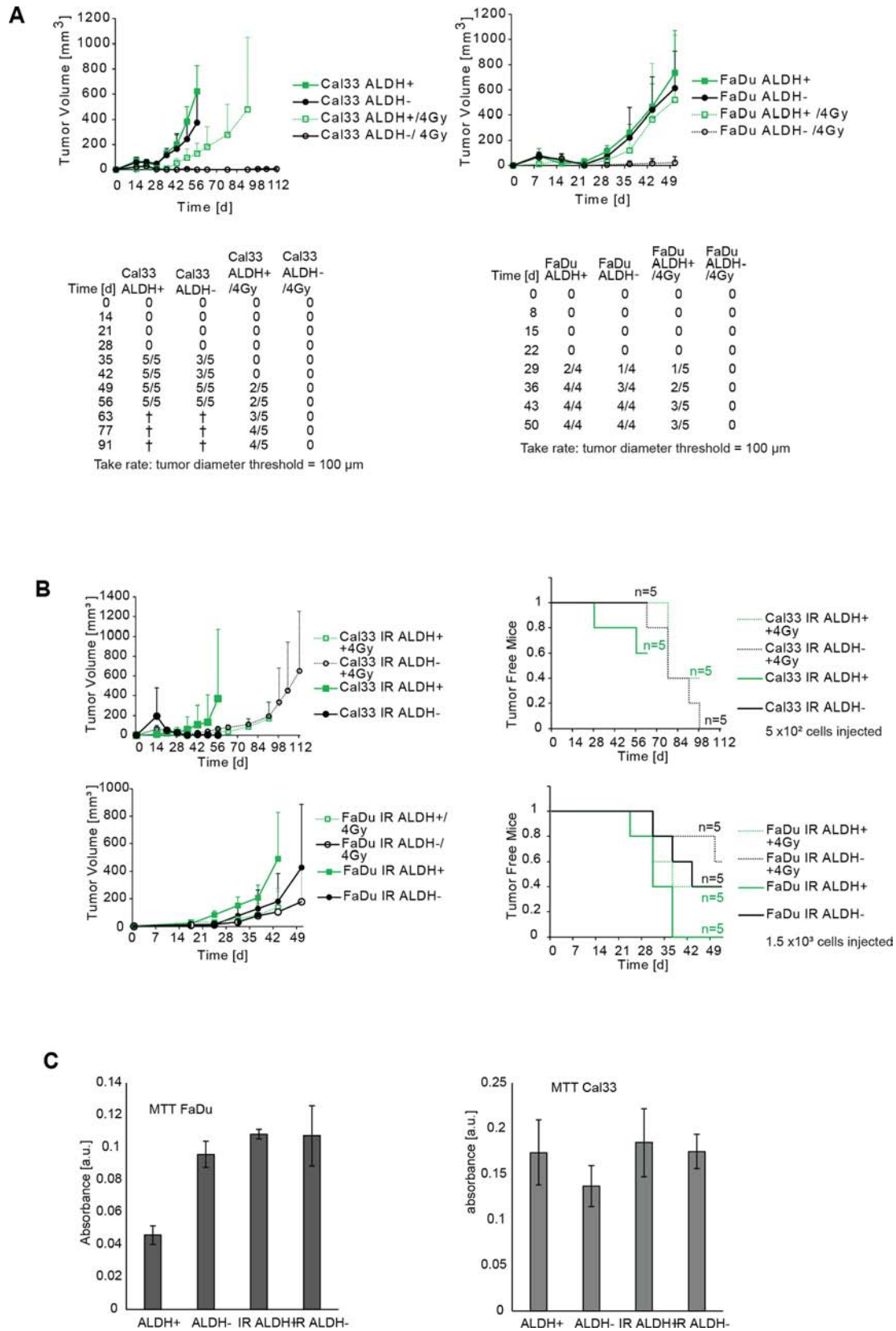
**Supplementary Figure S2: Putative cancer stem cell (CSC) marker expression at different time points after irradiation treatment.** A. flow cytometric analysis of the cell viability 24 h after the last irradiation fraction using DAPI staining. B. flow cytometric analysis of ALDH activity and CD133 surface expression after 0, 1, 3, 5 times 2 Gy of X-rays, measured 24 h and 7 d after the last irradiation fraction. C. Western blot analysis of Oct4 expression measured 7 d after the last dose.



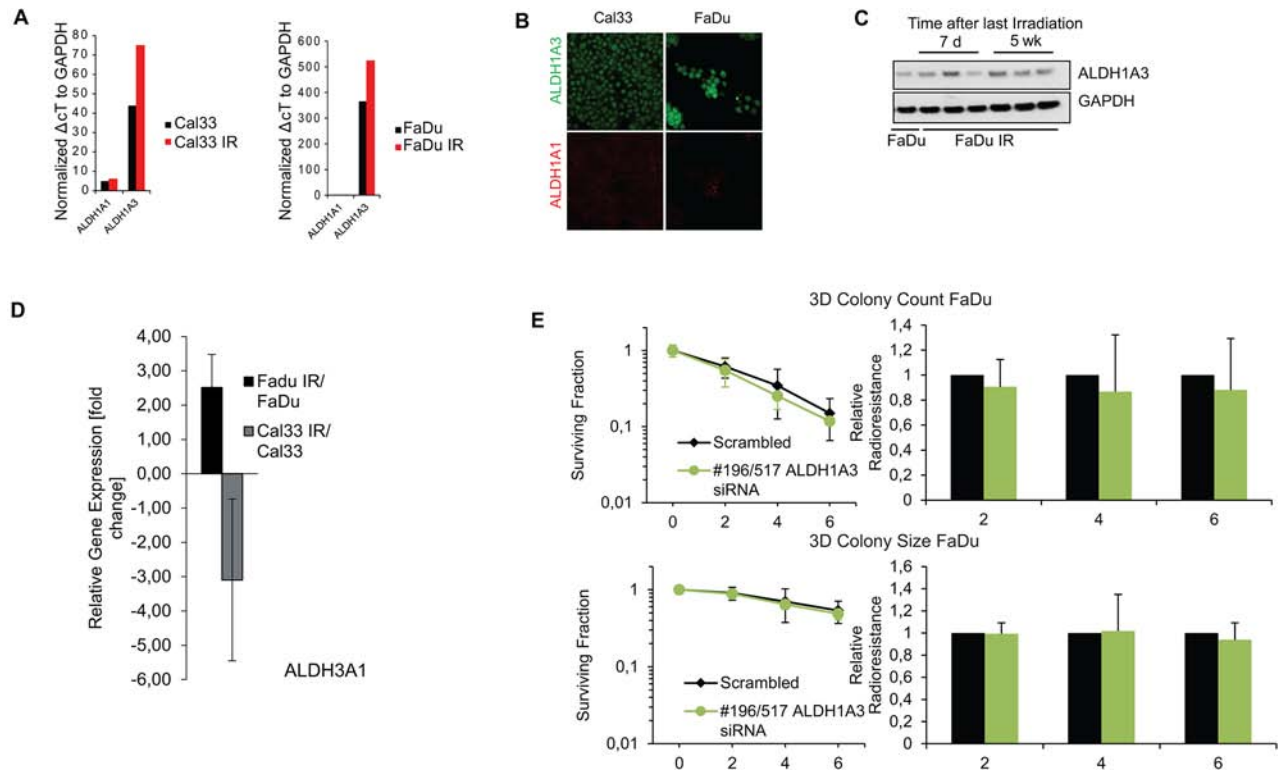
**Supplementary Figure S3: CSC protein expression levels upon irradiation.** A. quantification of the western blot from Figure 2B. B. quantification of the western blot from Figure 2C. C. Western blot analysis of FaDu IR subline analyzed at different timepoints after the last dose. D. quantification of the western blot from C. E. CSC protein changes upon irradiation in Cal33 and Cal33 IR. F. quantification of the western blot from F. (error bars = SD)



**Supplementary Figure S4: ALDH as a biomarker for radioresistance.** A. and B. Flow cytometric analysis of ALDH activity in Cal33 and FaDu C. absolute number of residual  $\gamma$ H2AX foci formed after 4 Gy of X-ray irradiation for ALDH<sup>+</sup> and ALDH<sup>-</sup> FaDu and Cal33 HNSCC lines. ( $p < 0,05$ , error bars = SD).



**Supplementary Figure S5: Tumor formation of ALDH populations from Cal33 and FaDu.** **A.** Tumorgrowth and up-take rates of Cal33 and FaDu ALDH<sup>+</sup> and ALDH<sup>-</sup> populations. **B.** Tumorgrowth Cal33 IR and FaDu IR ALDH<sup>+</sup> and ALDH<sup>-</sup> populations. **C.** Viability of ALDH sorted cells, which were injected into the mice. (error bars = SD).



**Supplementary Figure S6: Expression of ALDH1A3.** **A.** RT PCR of ALDH1A3 RNA expression in Cal33, FaDu, and their respective IR sublines. **B.** immunofluorescent analysis ALDH1A1 and ALDH1A3 expression. **C.** Western blot analysis of ALDH1A3 in FaDu IR sublines. **D.** Analysis of gene expression of the ALDH3A1 isozyme. **E.** Reduction of the ALDH1A3 expression by siRNA results in a slight increase in cell radiosensitivity of FaDu cells as compared to the siRNA control cells. ( $n = 3$ , error bars = SD).